Self-Assembly of Polymer-Tethered Nanorods

Mark A. Horsch,[1] Zhenli Zhang,[1] and Sharon C. Glotzer[1,2,*]

[1]*Department of Chemical Engineering, University of Michigan, Ann Arbor, Michigan 48109-2136, USA*
[2]*Department of Materials Science and Engineering, University of Michigan, Ann Arbor, Michigan 48109-2136, USA*

(Received 8 May 2005; published 29 July 2005)

We present results of molecular simulations that predict the phases formed by self-assembly of nanorods functionalized by a polymer "tether." Microphase separation of the immiscible tethers and rods coupled with the liquid crystal ordering of the rods induces the formation of a cubic phase, a smectic C phase, a tetragonally perforated lamellar phase, and a honeycomb phase; the latter two have been observed experimentally but have not been predicted. We also predict a new phase—a racemic mixture of hexagonally ordered chiral cylinders that self-assemble from these achiral building blocks.

DOI: 10.1103/PhysRevLett.95.056105 PACS numbers: 81.16.Dn, 81.07.−b, 83.80.Uv

Polymer-tethered nanoparticles constitute a class of "shape-amphiphiles"—geometric objects made of solvent-loving and solvent-hating parts [1]. These new materials have much in common with traditional molecular amphiphiles, but here the "head group" may be a hard particle of nanometer size. Under the right conditions, immiscibility between tether and nanoparticle and the geometric packing of the hard particles combine to produce complex self-assembled structures. Conventional rod-coil block copolymers are one limit of polymer-tethered rods (PTR), a specific class of polymer-tethered nanoparticles in which the nanoparticle is rodlike [2,3]. Various topologies of rod-coil block copolymers have been synthesized, with flexible polymers bonded to the middle or the end of the rod [4]. Rich morphologies arising from their self-assembly have been observed experimentally, e.g., layered smectic [5], wavy [5], and zigzag [6] lamellae, bicontinuous cubic structures [7], honeycombs [8,9], 3D tetragonally perforated lamellae [8,9], hexagonally packed cylinders [9], and hollow spherical and cylindrical micelles [10].

In contrast to block copolymers (BCPs) consisting of only flexible blocks, theoretical progress is less developed for rod-coil BCPs. Although the same principles govern the morphologies that form, the entropic interactions are more complicated in the latter due to the asymmetry between the two blocks and the tendency of the rigid block to orient itself relative to other rigid blocks as in molecular liquid crystals. Halperin and Semenov used scaling analysis to study the smectic A and smectic C phases [11,12], where the rods align parallel to the interfacial normal for smectic A and tilt with respect to the interfacial normal for smectic C. Williams and Fredrickson postulated the formation of pucklike micelles when the volume fraction of the coil is high [13]. Within the pucks, bundles of rods form a truncated cylindrical structure. In their study, the rods are assumed to be parallel to the cylinder axis, which may not represent the actual alignment due to the strong coupling between the stretching of the coil and the rod orientation. Holyst and others used a Landau free energy expansion in compositional and orientational order parameters to study the isotropic nematic transition and the smectic phases near the order disorder transition (ODT) [14]. Matsen and Barrett performed self-consistent field theory (SCFT) calculations on nematic and smectic rod-coil BCP phases [15] using Flory's lattice theory to incorporate orientational interactions. Pryamitsyn and Ganesan presented a SCFT model where the orientational interactions were included using Maier-Saupe interactions [16] and predicted the phase diagram for rod-coil BCPs for one and two dimensions. Kröger *et al.* [17] simulated rodlike particles with flexible tethers attached at opposing ends of the rod. Their studies focused on dynamics, ordering, and the effect of chain length and interaction strength on liquid and smectic phases.

In this study, we apply a coarse-grained, particle-based model [1] and use Brownian dynamics (BD) to study the phase behavior of a solution of tethered rods in three dimensions. The results of a solution of BCPs consisting of two flexible blocks are presented for comparison. A primary advantage of this model is that the liquid crystal behavior of the rods and the complex entropic interactions arising from the asymmetry between the rigid rods and the flexible polymer tethers are automatically incorporated. Another important feature is that our simulations are performed in three dimensions. Because of the coupling between orientational ordering and chain stretching, it is expected that the number of dimensions is significant in determining the final structures, especially the local packing of the rods. Our simulations demonstrate that tethered rods form structures not predicted by available theory, such as the honeycomb phase and the tetragonally perforated lamellar phase, which have been observed experimentally. We further predict the formation of a new phase comprised of chiral cylinders, which has not been previously reported in rod-coil BCP or related systems. This structure could serve as a new candidate to make biological or photosensitive sensors depending on the chemical nature of the PTR [18].

We model the rods as a series of N_A beads of species A linked rigidly in a linear geometry [1]. The polymer tethers are modeled as linear, bead-spring chains comprised of N_B beads of species B bonded together via a finitely extensi-

 © 2005 The American Physical Society

ble, nonlinear, elastic spring with a spring constant $k = 30$, and the maximum extendible length $R_0 = 1.5\sigma$; these values are chosen to prevent the tethers from crossing. To minimize computational requirements and allow for direct comparison to previous studies of flexible BCPs, we focus this study on tethered rods with equal numbers of beads, $N_A = N_B = 5$, in a selective solvent good for the tether and poor for the rods. Selectivity is incorporated by treating the solvophobic interactions between rods with an attractive Lennard-Jones potential with a cutoff radius $r_c = 2.5\sigma$ and the solvophilic interaction with a repulsive Weeks-Chandler-Andersen potential with a cutoff radius $r_c = 2^{1/6}\sigma$. The natural length and energy scales are σ and ε, respectively, with the time unit $\tau = \sigma\sqrt{m/\varepsilon}$, where m is the mass of a bead, σ is the diameter of a bead, and $\varepsilon = \varepsilon_{\mathrm{TT}} = \varepsilon_{\mathrm{PP}} = \varepsilon_{\mathrm{PT}}$. The inverse dimensionless temperature $1/T^*$ is ε/k_BT.

In BD, each bead is subjected to conservative, frictional, and random forces $\mathbf{F}_i^C$, $\mathbf{F}_i^F$, and $\mathbf{F}_i^R$, respectively, and its trajectory obeys the Langevin equation, $m\ddot{\mathbf{r}}_i = \mathbf{F}_i^C + \mathbf{F}_i^F + \mathbf{F}_i^R$ [19]. The frictional force is related to diffusion by the Einstein relation $\mathbf{F}_i^F = -\zeta\mathbf{v}_i = -k_BT/D\mathbf{v}_i$, where ζ is the friction coefficient (chosen to be $\zeta = 1.0\ \mathrm{m}\tau^{-1}$, thereby restricting the ballistic motion of a bead to $\sim 1\sigma$), $\mathbf{v}_i$ is the bead velocity, and D is the diffusivity. The random force $\mathbf{F}_i^R$ acts as a heat source and is calculated using $\langle \mathbf{F}_i^R(r)\mathbf{F}_j^R(t')\rangle = 6k_BT\zeta\delta_{ij}\delta(t - t')$. The rotational degrees of freedom of the rod are incorporated using equations of rotational motion for linear rigid bodies. The time step Δt used to integrate the discretized equations of motion is 0.01τ. All simulations are initially carried out in a cubic cell with periodic boundary conditions. For the tetragonally perforated lamellae and the honeycomb phases, the box search algorithm is also used, allowing the box to change shape [20]. Systems are initially equilibrated athermally and subsequently cooled to the target temperature. To avoid system size effects, we consider systems of 6000, 8000, 10 000, 13 000, and 20 000 particles.

The phase diagram (inverse temperature $1/T^*$ versus volume fraction $\phi = N\pi\sigma^3/6V_{\mathrm{box}}$) for a solution of tethered rods is presented in Fig. 1(a). For comparison the corresponding phase diagram of a solution of flexible BCPs is presented in Fig. 1(b). For the BCP system we predict the formation of the lamellar (L), hexagonal cylinder (H), and cubic (C) phases, which is consistent with theory and experiment. Monte Carlo simulations also predict the existence of the gyroid phase [21]. For the tethered nanorod system, we predict the formation of several complex phases described below.

Cubic micelle phase.—We observe a cubic micelle phase (C) for volume fractions between $\phi = 0.1$ and 0.17 [Fig. 2 (C)]. It is difficult to determine if the structures are bcc because of a nonuniform size distribution of the micelles. We do observe that, contrary to theoretical assumptions [13], the rods do not pack parallel within the micelles.

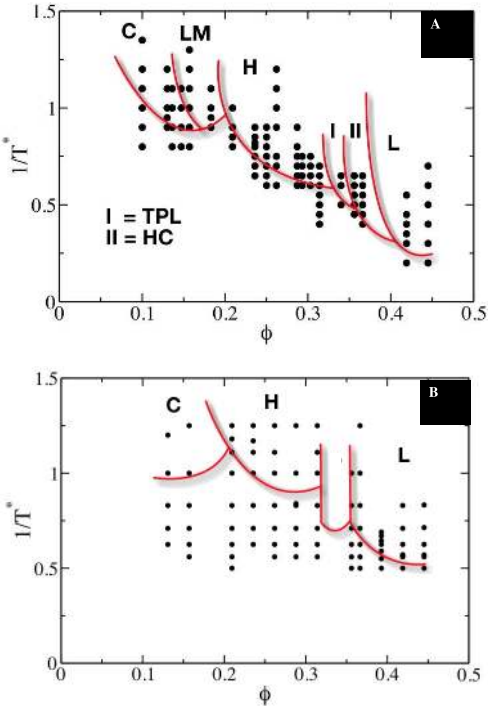

FIG. 1 (color online). (a) Phase diagram of P5T5 tethered rod. The solid lines are not actual phase boundaries but are visual guides separating the regions of the cubic micelle "C," long micelle "LM" (disordered cylindrical micelles), hexagonal cylinder "H," tetragonally perforated lamellar "TPL," honeycomb "HC," and lamellar morphologies "L." (b) Phase diagram of flexible BCPs for comparison. The region between the H and the L phases is expected to be the gyroid phase but requires additional simulations and remains to be verified.

Layered smectic C phase.—We observe a layered smectic C (lamellar) phase [Fig. 2 (L)] for volume fractions between $\phi = 0.36$ and 0.44 where the rods form a tilt angle with respect to the interfacial normal. The tilt angle arises due to a competition between the rods attempting to maximize their contact with other rods and the flexible tethers attempting to maximize their entropy [11,22]. The scaling analysis of Halperin predicts an increase in the tilt angle with an increase in temperature [22]. Our simulations quantitatively confirm the T dependence of the tilt angle in the smectic C phase. For example, we find that an increase in temperature from $T^* = 2.0$ to $T^* = 3.3$ results in an increase in the tilt angle from $\theta = 37°$ to $\theta = 43°$. Preliminary results from ongoing work suggest that the tether length may also be used to control the tilt angle by changing the volume occupied by the tether. Consistent with theory, previous simulations, and experiments [23–25], we observe an increase in T_{ODT} from $T^*_{\mathrm{ODT}} = 2.0$ for the flexible BCPs to $T^*_{\mathrm{ODT}} = 4.0$ for the tethered rods.

3D tetragonally perforated lamellar phase and honeycomb phase.—Our simulations predict that for $\phi = 0.31$–0.36 the tethered rods form 3D honeycomb (HC) and tetragonally perforated lamellar (TPL) phases [Fig. 2 (HC and TPL)]. Both of these structures have been re-

ported experimentally [8,9]. However, neither theory nor previous simulations have predicted the formation of these phases for PTR, presumably due to the assumptions of perfect ordering of the rigid rods, the initial guess of the candidate structure, or the small number of dimensions considered. These two complex 3D structures result from the competition between the rods attempting to maximize their contact with other rods to minimize energy and the tethers attempting to maximize their free volume to maximize entropy. As the volume fraction is lowered from that of the smectic C phase, the rods can rearrange to lower the grafting density of the flexible tethers. To accomplish this, the rods not only tilt with respect to the interfacial normal but they also reorient within the plane of the sheet. This allows for the formation of holes in the sheets that in turn reduces the tether grafting density, resulting in a decrease of the elastic energy of the tether and an increase in entropy. At high volume fractions, the holes form a hexagonal pattern, or honeycomb phase, the most efficient packing of circles within a 2D sheet. As the volume fraction is lowered, this restriction is somewhat mitigated and the PTR form 3D tetragonally perforated lamellar structures. The HC and TPL structures may be suitable candidates for negative refractive index materials [26]. We note that the holes in alternating sheets in the honeycomb and tetragonally perforated lamellar phases pack in an ABAB pattern.

Hexagonal chiral cylinder phase.—We observe a hexagonal cylinder (H) phase [Fig. 2 (H_I)] over a relatively broad region of the phase diagram, from $\phi = 0.2$ to $\phi = 0.31$. An H phase is predicted by theory and readily observed experimentally; however, our simulations predict a striking new feature not previously reported or predicted. We find the rods pack within the cylinders such that they induce a regular twist of period $\omega = 0.22 \pm 0.018$ about the cylinder axis, forming cylinders that are chiral nematic [Fig. 2 (H_I and H_{II})]. This is in contrast with previously assumed perfect parallel packing of the rods [27]. Radzilowski *et al.* [28] suggested that, if the rods pack in parallel or interdigitated bilayers or monolayers, they should form a square or rectangular cross section, which is not what they observed in the computer reconstructions of their data. They suggested that this could be due to the rod-coil junctions not being confined to a planar surface. The twists of the rods observed in our simulations do not restrict the rod tether junction to a planar surface, and as such the cross section is not square. Further evidence for this phase is demonstrated by the twisted ribbons observed in the work of Sone *et al.* [29], in which short rod-coil copolymers form long twisted ribbons that are not mesoscopically ordered.

Conventionally, chiral nematic structures form either from chiral building blocks or under the influence of an external field. The key to understanding how chirality arises in this system from the packing of building blocks that are, on average, achiral is again the competition between the interfacial energy and the elastic stretching energy of the flexible tethers. Halperin argued [11], and

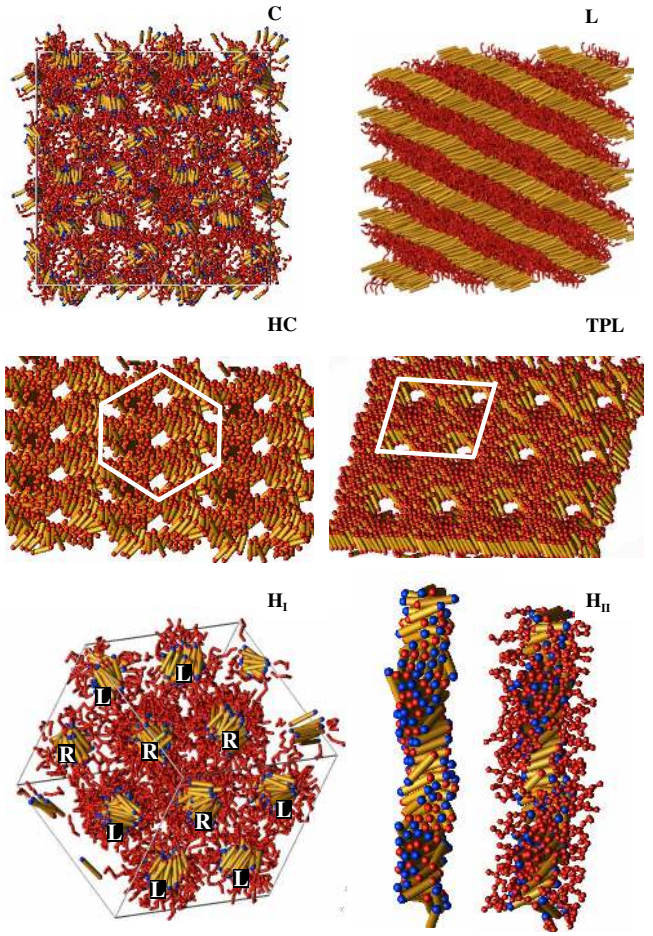

FIG. 2 (color online). Predicted morphologies of model tethered rods. (C) Cubic micelle phase. (L) Smectic C phase. (HC) Single sheet extracted from the honeycomb phase "HC." The rod ends are highlighted for viewing ease. (TPL) Single sheet extracted from the tetragonally perforated lamellar phase "TPL." Rod ends colored for viewing ease. (H_I) Hexagonal chiral cylinder phase "H," viewed on end. Cylinders are labeled "R" for right handedness and "L" for left handedness. The dark spheres represent rod ends with no tethers. (H_{II}) Individual chiral cylinder from hexagonal cylinder phase without tethers (left) with tethers (right). Lightly colored rod ends highlight a tether anchor point.

it has been shown experimentally [6], that for 2D sheets the rods form a tilt angle with respect to the interfacial normal. This is believed to arise from the fact that the effective grafting density is lowered by increasing the distance between the anchor points of neighboring tethers. This argument should also apply to the cylinder phase but with the addition of a second angle. In liquid crystals, where chiral phases form from chiral molecules, the molecules do not pack parallel to neighboring molecules, but instead assume a slight tilt angle [30]. Thus chirality in molecular liquid crystals is induced by a twist in the relative orientation of the chiral molecules, which propagates over macroscopic distances. In the tethered nanorod system, the tilt angle arises sterically, that is, for entropic

reasons associated with the excluded volume of the tether, inducing a twist that produces chiral self-assembled nanostructures. (Additional entropy is gained by the nanorods aligning such that the tether anchor point is randomly on one side or the other, thereby decreasing the local grafting density of the tether [Fig. 2 (H_{II})].)

Similar physics may underlie the recently discovered ''B2'' phase [31–34] comprised of achiral ''banana''-shaped molecules assembled into chiral domains [31–34]. In the experiments, oligomeric tails are linked to the end of the molecules, and the entropy of those tails may contribute to the tilt angle as they do in the simulations presented here. Thus, introducing functional groups or tethers to anisotropically shaped nanoparticles may provide a general method for creating chiral structures through self-assembly. We expect the bulkiness of the tether to play an important role in determining the pitch of the chiral structures [1].

The interplay between liquid crystal ordering and microphase separation can create new structures in self-assembled nanoparticle-based shape amphiphiles. For tethered nanorods, the competition between the interfacial energy and the elastic energy of the polymer tethers is key to understanding the various assemblies. Depending on the mesophases induced by microphase separation, this competition is manifested differently, resulting in a variety of structures. The success of this model in predicting experimentally observed structures that have not been predicted via theory suggests this simple model may be useful in predicting the phase behavior of polymer-tethered building blocks with more complicated topologies and geometries [1], and, in particular, may be useful in designing building blocks that can form chiral structures.

We thank R. D. Kamien, P. Palffy-Muhoray, R. G. Larson, C. Hall, A. Shultz, S. Fraden, S. I. Stupp, and C. R. Iacovella for helpful discussions. Financial support for this work was provided by the U.S. Department of Energy, Grant No. DE-FG02-02ER46000.

*Corresponding author.
Electronic address: sglotzer@umich.edu

[1] Z. L. Zhang, M. A. Horsch, M. H. Lamm, and S. C. Glotzer, Nano Lett. **3**, 1341 (2003).
[2] B. D. Busbee, S. O. Obare, and C. J. Murphy, Adv. Mater. **15**, 414 (2003).
[3] F. Shieh, A. E. Saunders, and B. A. Korgel, J. Phys. Chem. B **109**, 8538 (2005).
[4] C. Tschierske, J. Mater. Chem. **11**, 2647 (2001).
[5] J. W. Park and E. L. Thomas, Macromolecules **37**, 3532 (2004).
[6] J. T. Chen, E. L. Thomas, C. K. Ober, and S. S. Hwang, Macromolecules **28**, 1688 (1995).
[7] M. Lee, B. K. Cho, Y. S. Kang, and W. C. Zin, Macromolecules **32**, 7688 (1999).
[8] M. Lee *et al.*, J. Am. Chem. Soc. **123**, 4647 (2001).
[9] N. K. Oh, W. C. Zin, J. H. Im, J. H. Ryu, and M. Lee, Chem. Commun. (Cambridge) **04** (2004) 1092.
[10] S. A. Jenekhe and X. L. Chen, Science **279**, 1903 (1998).
[11] A. Halperin, Europhys. Lett. **10**, 549 (1989).
[12] A. N. Semenov and S. V. Vasilenko, Zh. Eksp. Teor. Fiz. **90**, 124 (1986).
[13] D. R. M. Williams and G. H. Fredrickson, Macromolecules **25**, 3561 (1992).
[14] R. Holyst and M. Schick, J. Chem. Phys. **96**, 730 (1992).
[15] M. W. Matsen and C. Barrett, Macromolecules **109**, 4108 (1998).
[16] V. Pryamitsyn and V. Ganesan, J. Chem. Phys. **120**, 5824 (2004).
[17] M. Kroger, Phys. Rep. **390**, 453 (2004).
[18] M. S. Spector, A. Singh, P. B. Messersmith, and J. M. Schnur, Nano Lett. **1**, 375 (2001).
[19] G. S. Grest and K. Kremer, Phys. Rev. A **33**, 3628 (1986).
[20] A. J. Schultz, C. K. Hall, and J. Genzer, J. Chem. Phys. **120**, 2049 (2004).
[21] R. G. Larson, J. Phys. II (France) **6**, 1441 (1996).
[22] A. Halperin, Macromolecules **23**, 2724 (1990).
[23] S. Lecommandoux, M. F. Achard, J. F. Langenwalter, and H. A. Klok, Macromolecules **34**, 9100 (2001).
[24] D. J. Pochan *et al.*, J. Polym. Sci., B Polym. Phys. **35**, 2629 (1997).
[25] F. S. Bates and G. H. Fredrickson, Annu. Rev. Phys. Chem. **41**, 525 (1990).
[26] M. Notomi, Phys. Rev. B **62**, 10 696 (2000).
[27] H. A. Klok and S. Lecommandoux, Adv. Mater. **13**, 1217 (2001).
[28] L. H. Radzilowski, B. O. Carragher, and S. I. Stupp, Macromolecules **30**, 2110 (1997).
[29] E. D. Sone, E. R. Zubarev, and S. I. Stupp, Angew. Chem., Int. Ed. **41**, 1705 (2002).
[30] R. D. Kamien and J. V. Selinger, J. Phys. Condens. Matter **13**, R1 (2001).
[31] A. Jakli, D. Kruerke, and G. G. Nair, Phys. Rev. E **67**, 051702 (2003).
[32] D. R. Link *et al.*, Science **278**, 1924 (1997).
[33] T. Niori, T. Sekine, J. Watanabe, T. Furukawa, and H. Takezoe, J. Mater. Chem. **6**, 1231 (1996).
[34] J. Xu, R. L. B. Selinger, J. V. Selinger, and R. Shashidhar, J. Chem. Phys. **115**, 4333 (2001).